

## Phase control of spin waves in the van der Waals antiferromagnet NiPS<sub>3</sub>

Shingo Toyoda<sup>1,2,\*</sup>, Jonathon Kruppe<sup>1,2,\*</sup>, Kohtaro Yamakawa,<sup>1,2</sup> James Analytis,<sup>1,2,3</sup> and Joseph Orenstein<sup>1,2</sup>

<sup>1</sup>*Department of Physics, University of California, Berkeley, California 94720, USA*

<sup>2</sup>*Materials Science Division, Lawrence Berkeley National Laboratory, Berkeley, California 94720, USA*

<sup>3</sup>*CIFAR Quantum Materials, CIFAR, Toronto, Ontario, Canada M5G 1M1*



(Received 14 September 2023; revised 29 November 2023; accepted 3 January 2024; published 8 February 2024)

We demonstrate phase control of magnons in the van der Waals antiferromagnet NiPS<sub>3</sub> using optical excitation by polarized light. The sign of the coherent precession of spin amplitude changes upon (i) reversing the helicity of a circularly polarized pump beam, or (ii) rotating the polarization of a linearly polarized pump by  $\pi/2$ . Because these two excitation pathways have comparable generation efficiency, the phase of spin precession can be continuously tuned from 0 to  $2\pi$  by controlling the polarization state of the pump pulse. The ability to excite magnons with a desired phase has potential applications in the design of a spin-wave phased array and ultrafast spin information processing.

DOI: [10.1103/PhysRevB.109.064408](https://doi.org/10.1103/PhysRevB.109.064408)

### I. INTRODUCTION

Coherent optical excitation of low energy collective modes is an important tool for both fundamental research and integration of materials into information technologies. One of the most prominent examples are magnons, the collective excitations of magnetic order [1–4]. Magnons in insulators can propagate over macroscopic distances without Joule heating, making them promising for energy-efficient computing [5]. While recent years have seen rapid advances in all-electrical control of incoherent magnons [5–8], these methods forego the potential of coherence. The phase information carried by coherent magnons provides an opportunity to design wave-based logic circuits that allow for non-Boolean computing, with the potential to operate faster and more efficiently than traditional Boolean logic circuits [9–12]. In another application, tuning the relative phase of an array of spin wave emitters allows control over the direction of wavefront propagation. This enables the creation of a “spin-wave phased-array antenna” which is desirable for spin based information processing [13,14].

While phase control of microwave-excited spin waves has been achieved through varying applied magnetic field [9] or microwave amplitude [15], such techniques are limited to ferromagnetic resonances within the gigahertz frequency range. Aiming at higher operation speeds, the focus of magnonics research is shifting from ferromagnetic materials toward antiferromagnets, which have the potential for terahertz bandwidth applications [16–18]. Two-dimensional (2D) van der Waals (vdW) antiferromagnets have attracted attention as they may serve as atomically thin magnonic devices [19–25]. Among them, the transition metal thiophosphates MPS<sub>3</sub> (*M*: Mn, Fe, Ni) are of particular interest because of their ultrafast spin dynamics [26–28]. While FePS<sub>3</sub> and MnPS<sub>3</sub> show easy-axis type antiferromagnetism [29–32], NiPS<sub>3</sub> is an *XY*-type easy-plane antiferromagnet [33–35], offering promise as a platform to explore 2D magnetic phenomena such as the

Berezinski-Kosterlitz-Thouless transition and long-distance spin transport via spin superfluidity [36,37].

Optical pump-probe methods are powerful tools to excite and detect picosecond time-scale spin dynamics, and a number of antiferromagnetic resonances have been detected using these techniques [26,27,38–44]. Despite this intense study, reports of phase control of optically excited spin waves are limited to ferromagnets, and in these reports only partial shifts in phase have been achieved [13,45]. Realizing full phase control from 0 to  $2\pi$  of light-induced antiferromagnetic magnons has remained a challenge.

In this Letter, we demonstrate full phase control of coherent magnon excitations in the vdW antiferromagnet NiPS<sub>3</sub>, achieved by varying the helicity of the pump photons. The unique feature of NiPS<sub>3</sub> that enables optical control of spin wave phase is the coexistence of two excitation mechanisms with comparable efficiency: one arising from linearly polarized (LP) light and the other from circular polarized (CP) light. In both cases the generation mechanism is fully coherent; the sign of the spin wave amplitude flips upon reversing circular polarization from left to right and rotating the linear polarization by  $\pi/2$ . This indicates that the excitation of magnons takes place through a nonthermal process, with the potential to control spin-wave phase via the light-matter interaction.

NiPS<sub>3</sub> crystallizes in a monoclinic structure with the space group *C2/m* [46–48]. The local magnetic moments are carried by the Ni<sup>2+</sup> ions. Trigonal distorted NiS<sub>6</sub> octahedra form an edge-sharing layered honeycomb lattice in the *ab* plane, see Fig. 1(a). The trigonal axis is perpendicular to the *ab* plane [49]. Below the Néel temperature  $T_N = 155$  K, Ni<sup>2+</sup> coplanar spins form ferromagnetic zig-zag chains along the *a* axis that are antiferromagnetically coupled along the *b* axis [Fig. 1(a)]. The easy plane is slightly tilted from basal plane [33–35]. In the following, we use Cartesian coordinates  $x \parallel a$ ,  $y \parallel b$ , and  $z \perp x, y$ .

The spin wave dynamics of such a biaxial antiferromagnet, in which spins are strongly confined to a plane and weakly oriented within that plane, is characterized by two magnon

\*These authors contributed equally to this work.

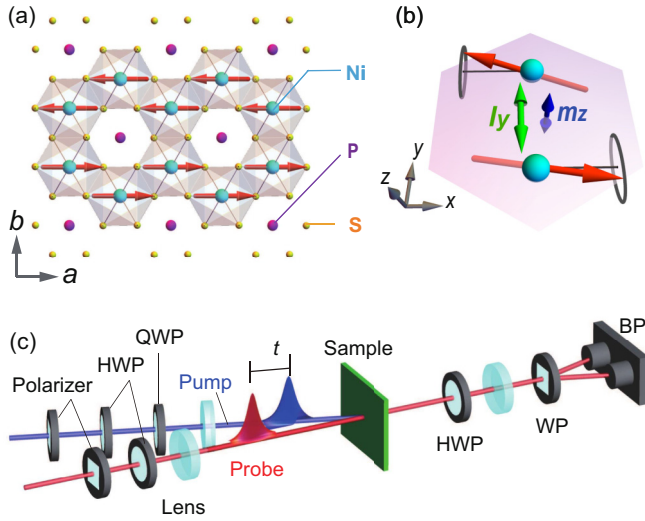


FIG. 1. (a) Crystal and magnetic structures of NiPS<sub>3</sub>. Red arrows indicate the magnetic moments of Ni<sup>2+</sup> ions. (b) Schematic illustration of the oscillations of the Ni<sup>2+</sup> spins (red arrows), Néel vector (green arrow), and magnetization (blue arrow) of the in-plane magnon mode. (c) Schematic diagram of the experimental setup for the optical pump-probe measurement. HWP, QWP, WP, and BP denote the half-wave plate, quarter-wave plate, Wollaston prism, and balanced photo detector, respectively.

modes [50]. In the lower frequency mode the Néel vector,  $L$  traces an ellipse with major axis in the magnetic easy plane [Fig. 1(b)] while the higher frequency mode, the major axis, is perpendicular to the easy plane. A previous pump-probe study of NiPS<sub>3</sub> showed that the lower frequency in-plane mode can be excited by a linearly polarized pump with a wavelength tuned to be resonant with a  $d-d$  transition of Ni<sup>2+</sup> [26].

## II. EXPERIMENTAL

We studied the dynamics of the in-plane mode of NiPS<sub>3</sub> as a function of photon polarization using the setup shown schematically in Fig. 1(c). The tunable light source is an optical parametric amplifier (OPA) pumped by a regeneratively amplified laser, producing 100 fs pulses at 5 kHz repetition rate. The OPA output, which was used as the pump, was tuned to 1240 nm to coincide with the  $d-d$  transition from the ground state  $^3A_{2g}$  to the excited state  $^3T_{2g}$  of Ni<sup>2+</sup> ions. The pump power was set to 2 mW and focused onto the sample with an approximate spot size of 100  $\mu\text{m}$ . The probe wavelength was 800 nm. The polarization rotation of the transmitted probe light was detected using a Wollaston prism and balanced photodetector.

Single crystals of NiPS<sub>3</sub> were grown by a chemical vapor transport method [51]. Stoichiometric amounts of Ni, P, and S were mixed and the resulting powder mixture was loaded in a quartz tube. The ampoule was heated at 800° (heating zone) and 700° (growth zone) for a week. The obtained crystals were characterized by powder x-ray diffraction and superconducting quantum interference device (SQUID) magnetometry, and then mechanically exfoliated on a copper substrate with a hole of diameter 500  $\mu\text{m}$ . The thickness of the sample was  $\sim 10$   $\mu\text{m}$ . The sample was mounted in a He closed-cycled refrigerator.

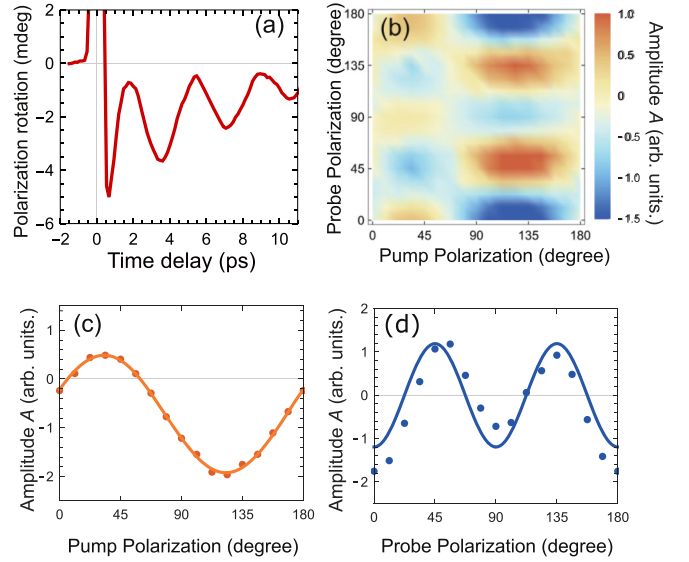


FIG. 2. (a) Time evolution of the probe polarization rotation for the linearly polarized pump measured at 12 K. (b) Probe and pump polarization dependence of the signed amplitude of linearly excited magnons in NiPS<sub>3</sub>. Negative values of the amplitude correspond to opposite phase from positive values. Spin precession amplitude as a function of (c) pump polarization for the fixed probe polarization angle at 0 degree. (d) Probe polarization dependence of the magnon amplitude for the pump polarization at 135 degrees. The solid lines are best fits.

## III. RESULTS AND DISCUSSION

We first measured the properties of magnon generation and detection with linearly polarized light. Figure 2(a) shows an example of photogenerated spin precession in NiPS<sub>3</sub> which can be fit to

$$\Phi(t) = A \exp(-t/\tau) \cos(\omega t + \eta) + P_2(t), \quad (1)$$

where  $A$ ,  $\omega$ ,  $\tau$ , and  $\eta$  are an amplitude, frequency, decay time, and initial phase of the oscillations, respectively.  $P_2(t)$  is a second-order polynomial that describes the smooth background on which the oscillations are superposed. Fitting gives the values of the magnon frequency  $\omega = 0.28$  THz with the lifetime  $\tau = 6$  ps. An overview of the dependence of the spin precession amplitude on pump and probe polarization is shown as a color map as a function of polarization of the pump and probe beams is shown as a color map in Fig. 2(b). First, we note that the dependence on polarization demonstrates that both the excitation and detection mechanisms is coherent, that is, magnons are generated and detected via a nonthermal light-matter interaction. Vertical and horizontal cuts through this plane clarify the dependence of  $A$  on polarization direction. The horizontal cut plotted in Fig. 2(c) shows  $A \propto \sin 2\theta$  at fixed probe angle, in this case  $\theta = 0^\circ$ . Finally, the vertical cut at fixed pump polarization  $\theta = 135^\circ$  shows that in this case  $A \propto \cos 4\theta$  [26,52]. Below we discuss how the dependence on the polarization of the pump and probe arise in an antiferromagnet with the symmetry of NiPS<sub>3</sub>.

In the phenomenological model of the light-matter interaction, the energy of the magneto-optical interaction is given by

[43,52–55]

$$\mathcal{W}_{MO} = -\frac{\chi_{ij}}{16\pi} \mathcal{E}_i \mathcal{E}_j^* \mathcal{T}(t), \quad (2)$$

where  $\mathcal{E}_i$  is the amplitude of the electric field of light. For light propagating in the  $z$  direction we consider the  $x$  and  $y$  components, which have the form  $\mathcal{E}_x \equiv \mathcal{E}_0 \cos \theta$  and  $\mathcal{E}_y \equiv \mathcal{E}_0 \sin \theta e^{i\xi}$ , respectively. Here  $\theta$  is the azimuthal angle of rotation about the  $z$  axis and  $\xi$  is the relative phase of the  $x$  and  $y$  components of the electric field. LP corresponds to  $\xi = 0$ , while CP corresponds to  $\xi = \pm\pi/2$ ,  $\theta = \pi/4$ . The time-dependent function  $\mathcal{T}(t)$  takes different forms depending on the type of excitation. For the displacive-type excitation [56,57], it is proportional to the Heaviside step function, while for the impulsive magnon excitation [43,52], it is proportional to Dirac delta function. The susceptibility tensor is given by  $\chi_{ij} = ik_{ijk}m_k + g_{ijkl}L_k l_n$  [52], where the lowercase  $l$  and  $m$  are the light-induced changes in the Néel vector and magnetization, respectively, and the  $L_k$  denote the components of the equilibrium Néel vector. When absorption is negligible, the Onsager reciprocity relation gives  $\chi_{ij}(m, l, L) = \chi_{ji}^*(m, l, L) = \chi_{ji}(-m, -l, -L)$ . Here we assume that this relation holds, because the pump and probe photon energies are below the parity-allowed charge transfer transition, leaving only the parity-forbidden weak  $d$ - $d$  transition. Consequently, the third rank axial tensor  $k_{ijk}$  and fourth rank polar tensor  $g_{ijkl}$  are purely real and satisfy  $k_{ijk} = -k_{jik}$  and  $g_{ijkl} = g_{jikl}$ . The tensor components that are relevant to the in-plane mode are  $k_{xyz} = -k_{yxz}$  and  $g_{xyxy} = g_{yxyx}$ , as the other components are either associated with the out-of-plane mode or vanish in the  $2/m$  point group (see the Supplemental Material [58]). The magneto-optical interaction energy of the lower frequency magnon mode can therefore be written as

$$\begin{aligned} \mathcal{W}_{MO} = & -\frac{I}{16\pi} \sin 2\theta [\mathcal{T}_m(t) k_{xyz} m_z \sin \xi \\ & + \mathcal{T}_l(t) g_{xyxy} L_x l_y \cos \xi], \end{aligned} \quad (3)$$

where  $I = \mathcal{E}_0 \mathcal{E}_0^*$  is proportional to the intensity of the pump light [ $l_y$  and  $m_z$  are sketched in Fig. 1(b)]. Equation (3) shows that the  $\sin(2\theta)$  dependence on pump polarization shown in Fig. 2 follows directly from the symmetry of NiPS<sub>3</sub>. Note that in addition to coupling via linearly polarized light ( $\xi = 0$ ) to fluctuations in  $l_y$ , coupling via circularly polarized light ( $\xi = \pi/2$ ) to  $m_z$  is allowed.

The detection of spin precession by the probe occurs via the inverse of the couplings described above and can arise from oscillations of  $l_y$  and/or  $m_z$ . Fluctuations in  $l_y$  give rise to magnetic linear birefringence, which has been shown [52] to manifest as the  $\cos 4\theta$  dependence on probe polarization that we observe [see Fig. 2(d)]. Fluctuations in  $m_z$  give rise to Faraday rotation which is independent of  $\theta$ . Hence, the detection of the in-plane magnon at the probe wavelength used in our measurements occurs via the magnetic linear birefringence associated with  $l_y$  rather than the Faraday rotation mediated by  $m_z$ .

Although the probe couples only  $l_y$ , the pump pulse can generate oscillations of both  $l_y$  and  $m_z$ , via coupling to linear and circular polarization, respectively. The key to phase control of spin precession in NiPS<sub>3</sub> is that both the LP and CP modes of magnon generation are not only nonzero, but

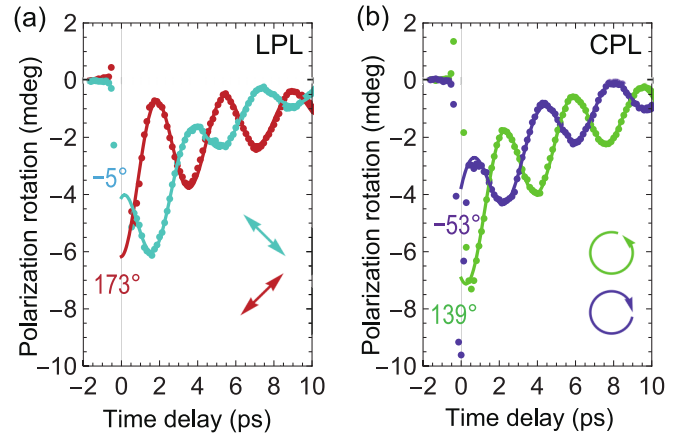


FIG. 3. Change in the probe polarization rotation as a function of time delay via the excitation of (a) linearly polarized light and (b) circularly polarized light at 12 K. The arrows schematically illustrate the polarization state of the pump pulses. The solid lines are the fits to Eq. (1). The initial phases of the magnon oscillation obtained from the fittings are also shown.

comparable in magnitude. This is illustrated in Figs. 3(a) and 3(b), which show time-resolved probe polarization rotation for LP and CP pump pulses, respectively, plotted on the same time and amplitude scales. The comparable magnitude of precession generated by LP and CP pump photons is notable, as in other systems the relative efficiency of magnon excitation varies by orders of magnitude [43,53]. The spin precession frequency  $\Omega$  is 0.28 THz for LP and 0.27 THz for CP, showing that the same spin wave mode is excited in both cases. Moreover, this frequency is consistent with the low-energy in-plane magnon mode found in the previous optical pump-probe [26] and electron spin resonance studies [59]. As illustrated in the inset of Fig. 3(a), the two responses to LP excitation shown are obtained by rotating the pump polarization by  $\pi/2$ ; the resulting  $\pi$  change in phase arises from the  $\sin 2\theta$  term in the light-matter interaction  $\mathcal{W}_{MO}$ . Figure 3(b) shows that the phase of the spin precession also changes by  $\pi$  for CP pumping upon reversing the helicity, arising in this case from the  $\sin \xi$  factor in  $\mathcal{W}_{MO}$ .

In addition to the sign reversal on changing polarization, Fig. 3 also displays the initial phase  $\eta$  for each of the curves. As we discuss below, the initial phase reflects the nature of the magnon generation mechanism [43,53,54]. The free energy of the easy-plane type antiferromagnet can be written as [26]

$$\begin{aligned} F = & \frac{1}{2M_0} \left( H_E \mathbf{M}^2 + \frac{H_x}{2} (M_x^2 + L_x^2) \right. \\ & \left. + \frac{H_z}{2} (M_z^2 + L_z^2) \right) + \mathcal{W}_{MO}, \end{aligned} \quad (4)$$

where  $H_E$  and  $H_{x,z}$  are the effective exchange field and anisotropy field, respectively. Dynamics described by Landau-Lifshitz equations,

$$\frac{d\mathbf{m}}{dt} = -\gamma \{ [\mathbf{M} \times \mathbf{H}^{\text{eff}}] + [\mathbf{L} \times \mathbf{h}^{\text{eff}}] \}, \quad (5)$$

$$\frac{d\mathbf{l}}{dt} = -\gamma \{ [\mathbf{M} \times \mathbf{h}^{\text{eff}}] + [\mathbf{L} \times \mathbf{H}^{\text{eff}}] \}, \quad (6)$$

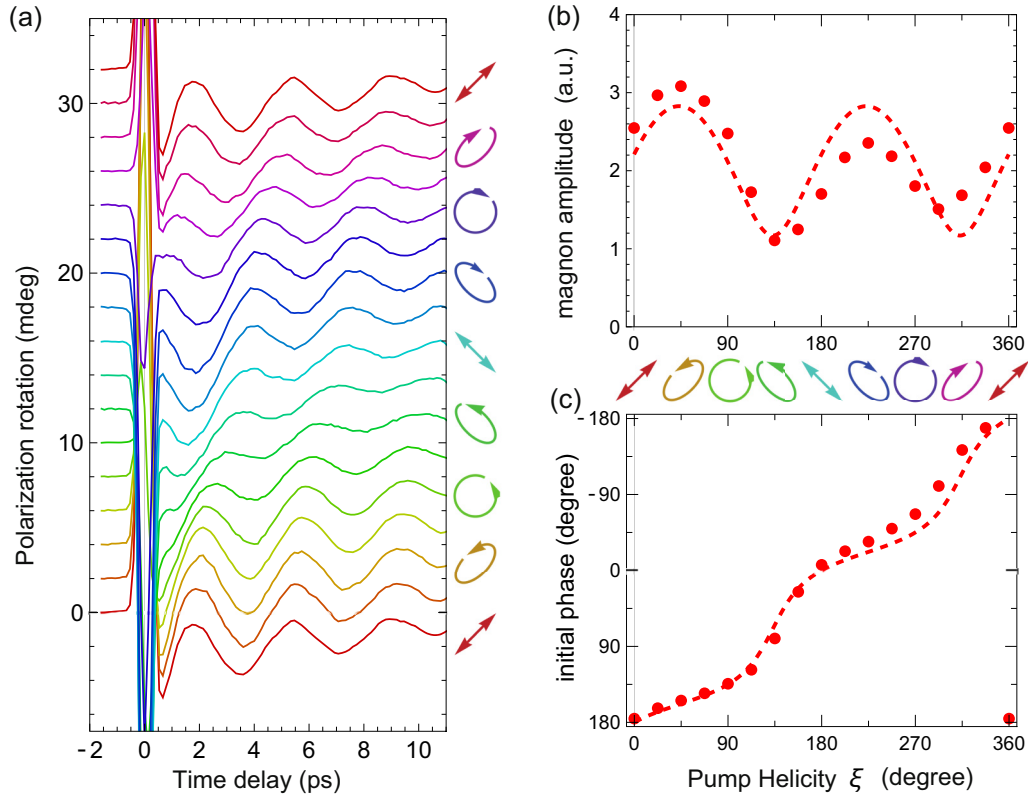


FIG. 4. (a) The time evolution of polarization rotation of the probe beam measured with varying polarization of the pump pulses at 12 K. The arrows schematically illustrate the polarization state of the pump. (b), (c) The pump polarization dependence of the (b) amplitude and (c) initial phase of the magnon oscillations. Dashed lines are fits to Eq. (10) and Eq. (11).

where  $\mathbf{H}^{\text{eff}} = -\partial F/\partial \mathbf{M}$  and  $\mathbf{h}^{\text{eff}} = -\partial F/\partial \mathbf{L}$ . Linearizing the equations leads to the following differential equations for the in-plane magnon mode:

$$\frac{dm_z}{\gamma dt} = -H_x l_y - h_l L_x \mathcal{T}_m(t), \quad (7)$$

$$\frac{dl_y}{\gamma dt} = H_0 m_z + h_m L_x \mathcal{T}_l(t), \quad (8)$$

where  $H_0 \equiv H_x - H_z - 2H_E$  and  $h_{m(l)} \equiv -\partial \mathcal{W}_{MO}/\partial m_z (\partial l_y)$ . Equations (7) and (8) describe spin oscillation at frequency  $\Omega = \gamma(H_0 H_x)^{1/2}$  with normal coordinate  $m_z = i(H_x/H_0)^{1/2} l_y$ . The phase of the oscillation after the pulsed excitation is determined by the torque functions,  $\mathcal{T}_{l,m}(t)$ . To illustrate the dynamics after pulsed excitation at  $t = 0$ , we consider the case of LP pump, where  $h_m = 0$ . For the impulsive generation mechanism  $\mathcal{T}(t) = \Delta t \delta(t)$  with  $\Delta t$  being the laser pulse duration, integrating the equations of motion gives  $m_z(t) = -\gamma h_l L_x \Delta t \cos \Omega t$ , whereas the displacive mechanism  $\mathcal{T}(t) = \Theta(t)$  yields  $m_z(t) = -\gamma h_l L_x \Omega^{-1} \sin \Omega t$ . Hence, LP pump induces  $\sin \Omega t$  ( $\cos \Omega t$ ) time dependence of  $l_y(t)$  for the impulsive (displacive) mechanism. In the case of excitation with CP light ( $h_l = 0$ ), Eqs. (7) and (8) predict  $l_y(t) \propto h_m \cos \Omega t$  and  $l_y(t) \propto h_m \sin \Omega t$  for impulsive and displacive excitation, respectively.

Our experimental results show cosinelike time dependence for the LP pump [Fig. 3(a)] while the CP pump induces a superposition of sine and cosine dependence [Fig. 3(b)] of  $l_y$ . This indicates that the displacive-type excitation plays

a dominant role for the LP pump, while both impulsive- and displacive-type excitation processes contribute to the generation of the in-plane magnon mode for CP pumping. Coexistence of impulsive and displacive excitation mechanisms have been observed previously in both coherent phonon excitation [60] and coherent magnon excitation [13].

With this understanding of the magnon generation and detection mechanisms, we turn to the demonstration of phase control shown in Fig. 4. The polarization of the pump beam is tuned continuously between LP and CP by transmission through a half-wave plate (HWP) and quarter-wave plate (QWP), as shown in Fig. 1(c). Varying the angle of the HWP, with the QWP fixed, continuously tunes the helicity  $\xi$  without changing the azimuthal angle  $\theta$ . Figure 4(a) shows time traces of the spin precession, for several  $\xi$  at  $\theta = 135^\circ$ . As the pump helicity is tuned, the phase of the oscillation shifts monotonically. Figures 4(b) and 4(c) display the phase and amplitude of the spin wave oscillation, obtained by fitting the traces to Eq. (1), as a function of pump helicity. Figure 4(b) demonstrates continuous tuning of the phase of the coherent magnon excitation from 0 to  $2\pi$ . The dashed lines through the data points are obtained by summing the contributions from the CP and LP components of the elliptical pump pulses. The probe polarization rotation can be described by

$$\Phi(t) = (A_{LP} \cos(\omega t + \eta_{LP}) \cos \xi + A_{CP} \cos(\omega t + \eta_{CP}) \sin \xi) \exp(-t/\tau), \quad (9)$$

where  $A_{LP}$  ( $A_{CP}$ ) and  $\eta_{LP}$  ( $\eta_{CP}$ ) denote the amplitude and initial phase for the case of the LP (CP) pump, respectively. The parameters  $\eta_{LP} = 180^\circ$  and  $\eta_{CP} = 140^\circ$  are obtained from measurements with pure LP and CP pump. Equation (9) yields a resultant helicity dependent magnon oscillation,  $A(\xi) \cos[\omega t + \eta(\xi)]e^{-t/\tau}$ , where

$$A(\xi) = \sqrt{A_{LP}^2 \cos^2 \xi + A_{CP}^2 \sin^2 \xi - 2A_{LP}A_{CP} \cos \xi \sin \xi \cos \eta_{CP}} \quad (10)$$

and

$$\eta(\xi) = \tan^{-1} \frac{A_{CP} \sin \xi \sin \eta_{CP}}{-A_{LP} \cos \xi + A_{CP} \sin \xi \cos \eta_{CP}}. \quad (11)$$

In principle, all magnetic systems in which magnons can be generated by both CP and LP light can manifest the phase control phenomenon described above. Indeed, both CP and LP excitation has been reported in other easy-plane type antiferromagnets, such as in FeBO<sub>3</sub> [43] and NiO [53]. However, magnon phase control was not demonstrated, likely due to the fact that the magnon excitation by LP light is approximately two orders of magnitude more efficient than excitation by CP light [43,53].

#### IV. CONCLUSION

To conclude, we performed time-resolved pump-probe measurements of the in-plane magnon mode in the antiferromagnet NiPS<sub>3</sub>. The amplitude of spin precession was comparable for LP and CP pump processes, yet their initial phase is different. By tuning the pump helicity, the phase of the spin oscillation shifts from 0 to  $2\pi$  with little change in amplitude, thus establishing a reliable scheme for magnon phase control in the ultrafast regime. This technique paves the way for the construction of magnon-based devices such as spin-wave logic circuits [9,10] and phased array [13,14]. Moreover, excitation of antiferromagnetic magnons can generate terahertz electromagnetic radiation [27], and thus control the magnon phase may be useful for example as terahertz phased array antennas.

#### ACKNOWLEDGMENTS

We acknowledge support from the Quantum Materials program under the Director, Office of Science, Office of Basic Energy Sciences, Materials Sciences and Engineering Division, of the U.S. Department of Energy, Contract No. DE-AC02-05CH11231. J.O. received support from the Gordon and Betty Moore Foundation's EPiQS Initiative through Grant GBMF4537 at UC Berkeley. S.T. is supported by JSPS Overseas Research Fellowships.

- 
- [1] V. Kruglyak, S. Demokritov, and D. Grundler, *Magnonics*, *J. Phys. D* **43**, 264001 (2010).
- [2] A. Barman, G. Gubbiotti, S. Ladak, A. O. Adeyeye, M. Krawczyk, J. Gräfe, C. Adelmann, S. Cotofana, A. Naemi, V. I. Vasyuchka *et al.*, The 2021 magnonics roadmap, *J. Phys.: Condens. Matter* **33**, 413001 (2021).
- [3] A. Kimel, A. Kirilyuk, P. Usachev, R. Pisarev, A. Balbashov, and T. Rasing, Ultrafast non-thermal control of magnetization by instantaneous photomagnetic pulses, *Nature (London)* **435**, 655 (2005).
- [4] C. D. Stanciu, F. Hansteen, A. V. Kimel, A. Kirilyuk, A. Tsukamoto, A. Itoh, and T. Rasing, All-optical magnetic recording with circularly polarized light, *Phys. Rev. Lett.* **99**, 047601 (2007).
- [5] Y. Kajiwara, K. Harii, S. Takahashi, J.-I. Ohe, K. Uchida, M. Mizuguchi, H. Umezawa, H. Kawai, K. Ando, K. Takanashi *et al.*, Transmission of electrical signals by spin-wave interconversion in a magnetic insulator, *Nature (London)* **464**, 262 (2010).
- [6] L. J. Cornelissen, J. Liu, R. A. Duine, J. B. Youssef, and B. J. van Wees, Long-distance transport of magnon spin information in a magnetic insulator at room temperature, *Nat. Phys.* **11**, 1022 (2015).
- [7] R. Lebrun, A. Ross, S. A. Bender, A. Qaiumzadeh, L. Baldrati, J. Cramer, A. Brataas, R. A. Duine, and M. Kläui, Tunable long-distance spin transport in a crystalline antiferromagnetic iron oxide, *Nature (London)* **561**, 222 (2018).
- [8] R. Lebrun, A. Ross, O. Gomonay, V. Baltz, U. Ebels, A. L. Barra, A. Qaiumzadeh, A. Brataas, J. Sinova, and M. Kläui, Long-distance spin-transport across the morin phase transition up to room temperature in ultra-low damping single crystals of the antiferromagnet  $\alpha$ -Fe<sub>2</sub>O<sub>3</sub>, *Nat. Commun.* **11**, 6332 (2020).
- [9] T. Schneider, A. A. Serga, B. Leven, B. Hillebrands, R. L. Stamps, and M. P. Kostylev, Realization of spin-wave logic gates, *Appl. Phys. Lett.* **92**, 022505 (2008).
- [10] M. Kostylev, A. Serga, T. Schneider, B. Leven, and B. Hillebrands, Spin-wave logical gates, *Appl. Phys. Lett.* **87**, 153501 (2005).
- [11] A. V. Chumak, V. I. Vasyuchka, A. A. Serga, and B. Hillebrands, Magnon spintronics, *Nat. Phys.* **11**, 453 (2015).
- [12] G. Csaba, A. Papp, and W. Porod, Spin-wave based realization of optical computing primitives, *J. Appl. Phys.* **115**, 17C741 (2014).
- [13] I. Yoshimine, T. Satoh, R. Iida, A. Stupakiewicz, A. Maziewski, and T. Shimura, Phase-controllable spin wave generation in iron garnet by linearly polarized light pulses, *J. Appl. Phys.* **116**, 043907 (2014).
- [14] M. Song, K.-W. Moon, C. Hwang, and K.-J. Kim, Omnidirectional spin-wave array antenna, *Phys. Rev. Appl.* **11**, 024027 (2019).
- [15] A. B. Ustinov, B. A. Kalinikos, and E. Lähderanta, Nonlinear phase shifters based on forward volume spin waves, *J. Appl. Phys.* **113**, 113904 (2013).
- [16] T. Jungwirth, X. Marti, P. Wadley, and J. Wunderlich, Antiferromagnetic spintronics, *Nat. Nanotechnol.* **11**, 231 (2016).
- [17] V. Baltz, A. Manchon, M. Tsoi, T. Moriyama, T. Ono, and Y. Tserkovnyak, Antiferromagnetic spintronics, *Rev. Mod. Phys.* **90**, 015005 (2018).
- [18] P. Němec, M. Fiebig, T. Kampfrath, and A. V. Kimel, Antiferromagnetic opto-spintronics, *Nat. Phys.* **14**, 229 (2018).

- [19] B. Huang, G. Clark, E. Navarro-Moratalla, D. R. Klein, R. Cheng, K. L. Seyler, D. Zhong, E. Schmidgall, M. A. McGuire, D. H. Cobden *et al.*, Layer-dependent ferromagnetism in a van der Waals crystal down to the monolayer limit, *Nature (London)* **546**, 270 (2017).
- [20] C. Gong, L. Li, Z. Li, H. Ji, A. Stern, Y. Xia, T. Cao, W. Bao, C. Wang, Y. Wang *et al.*, Discovery of intrinsic ferromagnetism in two-dimensional van der Waals crystals, *Nature (London)* **546**, 265 (2017).
- [21] Z. Fei, B. Huang, P. Malinowski, W. Wang, T. Song, J. Sanchez, W. Yao, D. Xiao, X. Zhu, A. F. May *et al.*, Two-dimensional itinerant ferromagnetism in atomically thin  $\text{Fe}_3\text{GeTe}_2$ , *Nat. Mater.* **17**, 778 (2018).
- [22] X. Cai, T. Song, N. P. Wilson, G. Clark, M. He, X. Zhang, T. Taniguchi, K. Watanabe, W. Yao, D. Xiao *et al.*, Atomically thin  $\text{CrCl}_3$ : An in-plane layered antiferromagnetic insulator, *Nano Lett.* **19**, 3993 (2019).
- [23] G. Long, H. Henck, M. Gibertini, D. Dumcenco, Z. Wang, T. Taniguchi, K. Watanabe, E. Giannini, and A. F. Morpurgo, Persistence of magnetism in atomically thin  $\text{MnPS}_3$  crystals, *Nano Lett.* **20**, 2452 (2020).
- [24] Y. Khan, S. M. Obaidulla, M. R. Habib, A. Gayen, T. Liang, X. Wang, and M. Xu, Recent breakthroughs in two-dimensional van der Waals magnetic materials and emerging applications, *Nano Today* **34**, 100902 (2020).
- [25] M.-C. Wang, C.-C. Huang, C.-H. Cheung, C.-Y. Chen, S. G. Tan, T.-W. Huang, Y. Zhao, Y. Zhao, G. Wu, Y.-P. Feng *et al.*, Prospects and opportunities of 2d van der Waals magnetic systems, *Ann. Phys.* **532**, 1900452 (2020).
- [26] D. Afanasiev, J. R. Hortensius, M. Matthiesen, S. Mañas-Valero, M. Šiškins, M. Lee, E. Lesne, H. S. van Der Zant, P. G. Steeneken, B. A. Ivanov *et al.*, Controlling the anisotropy of a van der Waals antiferromagnet with light, *Sci. Adv.* **7**, eabf3096 (2021).
- [27] C. A. Belvin, E. Baldini, I. O. Ozel, D. Mao, H. C. Po, C. J. Allington, S. Son, B. H. Kim, J. Kim, I. Hwang *et al.*, Exciton-driven antiferromagnetic metal in a correlated van der Waals insulator, *Nat. Commun.* **12**, 4837 (2021).
- [28] F. Mertens, D. Mönkebüscher, U. Parlak, C. Boix-Constant, S. Mañas-Valero, M. Matzer, R. Adhikari, A. Bonanni, E. Coronado, A. M. Kalashnikova *et al.*, Ultrafast coherent THz lattice dynamics coupled to spins in the van der Waals antiferromagnet  $\text{FePS}_3$ , *Adv. Mater.* **35**, 2208355 (2022).
- [29] D. Lançon, H. C. Walker, E. Ressouche, B. Ouladdiaf, K. C. Rule, G. J. McIntyre, T. J. Hicks, H. M. Rønnow, and A. R. Wildes, Magnetic structure and magnon dynamics of the quasi-two-dimensional antiferromagnet  $\text{FePS}_3$ , *Phys. Rev. B* **94**, 214407 (2016).
- [30] N. Chandrasekharan and S. Vasudevan, Magnetism, exchange and crystal field parameters in the orbitally unquenched ising antiferromagnet  $\text{FePS}_3$ , *Pramana* **43**, 21 (1994).
- [31] K. Kurosawa, S. Saito, and Y. Yamaguchi, Neutron diffraction study on  $\text{MnPS}_3$  and  $\text{FePS}_3$ , *J. Phys. Soc. Jpn.* **52**, 3919 (1983).
- [32] E. Ressouche, M. Loire, V. Simonet, R. Ballou, A. Stunault, and A. Wildes, Magnetoelectric  $\text{MnPS}_3$  as a candidate for ferrotoroidicity, *Phys. Rev. B* **82**, 100408(R) (2010).
- [33] P. A. Joy and S. Vasudevan, Magnetism in the layered transition-metal thiophosphates  $\text{MPS}_3$  ( $M = \text{Mn, Fe, and Ni}$ ), *Phys. Rev. B* **46**, 5425 (1992).
- [34] A. R. Wildes, V. Simonet, E. Ressouche, G. J. McIntyre, M. Avdeev, E. Suard, S. A. Kimber, D. Lançon, G. Pepe, B. Moubaraki, T. J. Hicks, Magnetic structure of the quasi-two-dimensional antiferromagnet  $\text{NiPS}_3$ , *Phys. Rev. B* **92**, 224408 (2015).
- [35] K. Kim, S. Y. Lim, J.-U. Lee, S. Lee, T. Y. Kim, K. Park, G. S. Jeon, C.-H. Park, J.-G. Park, and H. Cheong, Suppression of magnetic ordering in XXZ-type antiferromagnetic monolayer  $\text{NiPS}_3$ , *Nat. Commun.* **10**, 345 (2019).
- [36] U. F. P. Seifert, M. Ye, and L. Balents, Ultrafast optical excitation of magnetic dynamics in van der Waals magnets: Coherent magnons and BKT dynamics in  $\text{NiPS}_3$ , *Phys. Rev. B* **105**, 155138 (2022).
- [37] S. Takei, B. I. Halperin, A. Yacoby, and Y. Tserkovnyak, Superfluid spin transport through antiferromagnetic insulators, *Phys. Rev. B* **90**, 094408 (2014).
- [38] T. Satoh, S.-J. Cho, R. Iida, T. Shimura, K. Kuroda, H. Ueda, Y. Ueda, B. A. Ivanov, F. Nori, and M. Fiebig, Spin oscillations in antiferromagnetic  $\text{NiO}$  triggered by circularly polarized light, *Phys. Rev. Lett.* **105**, 077402 (2010).
- [39] D. Bossini, S. Dal Conte, Y. Hashimoto, A. Secchi, R. V. Pisarev, T. Rasing, G. Cerullo, and A. V. Kimel, Macrospin dynamics in antiferromagnets triggered by sub-20 femtosecond injection of nanomagnons, *Nat. Commun.* **7**, 10645 (2016).
- [40] T. Satoh, R. Iida, T. Higuchi, M. Fiebig, and T. Shimura, Writing and reading of an arbitrary optical polarization state in an antiferromagnet, *Nat. Photon.* **9**, 25 (2015).
- [41] S. Baierl, M. Hohenleutner, T. Kampfrath, A. Zvezdin, A. V. Kimel, R. Huber, and R. Mikhaylovskiy, Nonlinear spin control by terahertz-driven anisotropy fields, *Nat. Photon.* **10**, 715 (2016).
- [42] A. M. Kalashnikova, A. V. Kimel, R. V. Pisarev, V. N. Gridnev, A. Kirilyuk, and T. Rasing, Impulsive generation of coherent magnons by linearly polarized light in the easy-plane antiferromagnet  $\text{FeBO}_3$ , *Phys. Rev. Lett.* **99**, 167205 (2007).
- [43] A. M. Kalashnikova, A. V. Kimel, R. V. Pisarev, V. N. Gridnev, P. A. Usachev, A. Kirilyuk, and T. Rasing, Impulsive excitation of coherent magnons and phonons by subpicosecond laser pulses in the weak ferromagnet  $\text{FeBO}_3$ , *Phys. Rev. B* **78**, 104301 (2008).
- [44] X.-X. Zhang, L. Li, D. Weber, J. Goldberger, K. F. Mak, and J. Shan, Gate-tunable spin waves in antiferromagnetic atomic bilayers, *Nat. Mater.* **19**, 838 (2020).
- [45] A. I. Chernov, M. A. Kozhaev, A. Khramova, A. N. Shaposhnikov, A. R. Prokopov, V. N. Berzhansky, A. K. Zvezdin, and V. I. Belotelov, Control of the phase of the magnetization precession excited by circularly polarized femtosecond-laser pulses, *Photonics Res.* **6**, 1079 (2018).
- [46] M. Bernasconi, G. L. Marra, G. Benedek, L. Miglio, M. Jouanne, C. Julien, M. Scagliotti, and M. Balkanski, Lattice dynamics of layered  $\text{MPX}_3$  ( $M = \text{mn, Fe, Ni, Zn}$ ;  $X = \text{S, Se}$ ) compounds, *Phys. Rev. B* **38**, 12089 (1988).
- [47] R. Brec, Review on structural and chemical properties of transition metal phosphorus trisulfides  $\text{MPS}_3$ , *Solid State Ionics* **22**, 3 (1986).
- [48] G. Ouvrard, R. Brec, and J. Rouxel, Structural determination of some  $\text{MPS}_3$  layered phases ( $M = \text{Mn, Fe, Co, Ni}$  and  $\text{Cd}$ ), *Mater. Res. Bull.* **20**, 1181 (1985).

- [49] A. R. Wildes, J. R. Stewart, M. D. Le, R. A. Ewings, K. C. Rule, G. Deng, and K. Anand, Magnetic dynamics of NiPS<sub>3</sub>, *Phys. Rev. B* **106**, 174422 (2022).
- [50] S. M. Rezende, A. Azevedo, and R. L. Rodríguez-Suárez, Introduction to antiferromagnetic magnons, *J. Appl. Phys.* **126**, 151101 (2019).
- [51] C.-H. Ho, T.-Y. Hsu, and L. C. Muhimma, The band-edge excitons observed in few-layer NiPS<sub>3</sub>, *npj 2D Materials and Applications* **5**, 8 (2021).
- [52] T. Satoh, R. Iida, T. Higuchi, Y. Fujii, A. Koreeda, H. Ueda, T. Shimura, K. Kuroda, V. Butrim, and B. Ivanov, Excitation of coupled spin-orbit dynamics in cobalt oxide by femtosecond laser pulses, *Nat. Commun.* **8**, 638 (2017).
- [53] C. Tzschaschel, K. Otani, R. Iida, T. Shimura, H. Ueda, S. Günther, M. Fiebig, and T. Satoh, Ultrafast optical excitation of coherent magnons in antiferromagnetic NiO, *Phys. Rev. B* **95**, 174407 (2017).
- [54] V. N. Gridnev, Phenomenological theory for coherent magnon generation through impulsive stimulated Raman scattering, *Phys. Rev. B* **77**, 094426 (2008).
- [55] P. Pershan, J. Van der Ziel, and L. Malmstrom, Theoretical discussion of the inverse Faraday effect, Raman scattering, and related phenomena, *Phys. Rev.* **143**, 574 (1966).
- [56] F. Hansteen, A. Kimel, A. Kirilyuk, and T. Rasing, Nonthermal ultrafast optical control of the magnetization in garnet films, *Phys. Rev. B* **73**, 014421 (2006).
- [57] F. Atoneche, A. M. Kalashnikova, A. V. Kimel, A. Stupakiewicz, A. Maziewski, A. Kirilyuk, and T. Rasing, Large ultrafast photoinduced magnetic anisotropy in a cobalt-substituted yttrium iron garnet, *Phys. Rev. B* **81**, 214440 (2010).
- [58] See Supplemental Material at <http://link.aps.org/supplemental/10.1103/PhysRevB.109.064408> for the details of the antiferromagnetic spin dynamics; light-matter interaction; magnon detection scheme; and static birefringence measurement.
- [59] K. Mehlawat, A. Alfonsov, S. Selzer, Y. Shemerliuk, S. Aswartham, B. Büchner, and V. Kataev, Low-energy excitations and magnetic anisotropy of the layered van der Waals antiferromagnet Ni<sub>2</sub>P<sub>2</sub>S<sub>6</sub>, *Phys. Rev. B* **105**, 214427 (2022).
- [60] G. A. Garrett, T. F. Albrecht, J. F. Whitaker, and R. Merlin, Coherent THz phonons driven by light pulses and the sb problem: What is the mechanism? *Phys. Rev. Lett.* **77**, 3661 (1996).